Citation
Sheppard, D.A. and Paskevicius, M. and Javadian, P. and Davies, I.J. and Buckley, C.E. 2019. Methods for accurate high-temperature Sieverts-type hydrogen measurements of metal hydrides. Journal of Alloys and Compounds. 787: pp. 1225-1237.
http://doi.org/10.1016/j.jallcom.2019.02.067

Methods for accurate high-temperature Sieverts-type hydrogen measurements of metal hydrides

Drew A. Sheppard*[1], Mark Paskevicius[1], Payam Javadian[1], Ian J. Davies[2], Craig E. Buckley[1]

[1] *Hydrogen Storage Research Group, Fuels and Energy Technology Institute, Department of Physics, Curtin University, GPO Box U1987, Perth, WA 6845, Australia.*

[2] *School of Civil and Mechanical Engineering*, Curtin University, Perth, WA 6845, Australia.

E-mail addresses: drew.sheppard@gmail.com (D. Sheppard), mark.paskevicius@gmail.com (M. Paskevicius), payam_javadian@hotmail.com (P. Javadian), i.davies@curtin.edu.au (I. Davies), c.buckley@curtin.edu.au (C. Buckley).

Keywords: Sieverts apparatus, hydrogen permeability, hydrogen solubility, metal hydrides, thermodynamic properties, gas-solid reactions.

Abstract:

The potential of high-temperature metal hydrides (HTMHs) as thermal energy storage materials means that accurate assessment of their properties are required on the laboratory scale. Above ≃ 450 °C, the hydrogen permeability of sample cell reactors (SCRs) used in experiments to characterise HTMHs can have an appreciable impact on the data. In this work, the thermodynamic and kinetic properties of TiH_x have been measured at temperatures up to 725 °C as a test of different practical methods for limiting the effects of hydrogen permeability and solubility in SCRs during high-temperature characterisation of metal hydrides. Aluminium-coated stainless steel and α-SiC were used to construct SCRs with reduced hydrogen permeability using commercially available techniques. When steel SCRs are the only practical option, guidelines have been developed to choose experimental conditions that minimise the effect on the data collected due to their hydrogen permeability and solubility. A method has also been developed to correct collected data for the hydrogen permeability and solubility of SCRs.

List of Abbreviations and Symbols

HTMH	= High-temperature metal hydride
TES	= Thermal energy storage
SCR	= Sample cell reactor
CSP	= Concentrating solar power
PCI	= pressure-composition-isotherm
H/M	= (atomic) hydrogen to metal ratio
OD	= outer diameter
ID	= inner diameter
SS	= stainless steel
χ	= equilibrium concentration of dissolved H_2 in SS that is exposed to a uniform gas pressure (mol $H_2 \cdot m^{-3}$).
$\Delta\chi$	= equilibrium concentration gradient of dissolved H_2 in a SS plate that supports a pressure difference (mol $H_2 \cdot m^{-3}$).
V^{SS}	= volume of SS exposed to a uniform H_2 gas pressure (m^3).
V^{SCR}	= volume of SS in a SCR exposed to a pressure differential (m^3).
m^{SS}	= mass of SS exposed to a uniform H_2 gas pressure (kg).
m^{SCR}	= mass of the SS SCR exposed to a H_2 gas pressure differential (kg).
ρ^{SS}	= density of SS exposed to a uniform H_2 gas pressure ($kg \cdot m^{-3}$).
ρ^{SCR}	= density of the SS SCR exposed to a pressure differential ($kg \cdot m^{-3}$).

f = H_2 gas fugacity (MPa).
P = H_2 gas pressure (MPa).
Z = compressibility of H_2 to account for the deviation from ideal gas behaviour.
T = temperature (K).
R = gas constant (8.3144598 J·mol^{-1}·K^{-1}).
K = temperature dependant solubility of H_2 (mol H_2·m^{-3}·MPa$^{-1/2}$) .
K_o = solubility pre-exponential factor (mol H_2·m^{-3}·MPa$^{-1/2}$).
ΔH_s = heat of formation of atomic hydrogen in steel (J·mol H^{-1}).
SA = internal surface area of SS exposed to H_2 gas (m^2).
J_∞ = steady state diffusional flux of H_2 (mol H_2·m^{-2}·s^{-1}).
s = measurement duration (s).
t = thickness of SS plate (m).
Φ = temperature dependent permeability of H_2 (mol H_2·m^{-1}·s^{-1}·MPa$^{-1/2}$).
Φ_o = permeability pre-exponential factor (mol H_2·m^{-1}·s^{-1}·MPa$^{-1/2}$).
H_Φ = permeability activation energy of atomic hydrogen (J·mol H^{-1}).
$(SA/t)_{\text{eff}}$ = a single variable based on the geometry of the SCR (m).
$n(\mathrm{H_2})_{\mathrm{MH}}$ = moles of H_2 in the metal hydride sample.
$n(\mathrm{H_2})_{\mathrm{gas}}$ = moles of H_2 in the gas phase within the Sieverts-type instrument.
$n(\mathrm{H_2})_{\Phi}^{\mathrm{SCR\ calc.}}$ = calculated moles of H_2 permeated by the SCR (mol H_2).
$n(\mathrm{H_2})_{\Phi}^{\mathrm{SCR\ meas.}}$ = measured moles of H_2 absorbed/desorbed by the SCR (mol H_2).
$n(\mathrm{H_2})_{\chi}^{\mathrm{SS}}$ = moles of H_2 gas dissolved in SS exposed to a uniform gas pressure (mol H_2).
$n(\mathrm{H_2})_{\Delta\chi}^{\mathrm{SCR}}$ = moles of H2 gas dissolved in a SS plate exposed to a H_2 gas pressure differential (mol H_2).
i = counting index for i^{th} measurement.
N = superscript indicating summation over all i measurements.

Example usage of superscripts:

$n^{i}(\mathrm{H_2})_{\mathrm{MH}}$ = moles of H_2 in the metal hydride sample after the i^{th} measurement.
$n^{i-1}(\mathrm{H_2})_{\mathrm{MH}}$ = moles of H_2 in the metal hydride sample after the i^{th} – 1 measurement.
$n^{N}(\mathrm{H_2})_{\mathrm{MH}}$ = cumulative moles of H_2 absorbed/desorbed by the metal hydride sample after N data measurement steps.
$\Delta n^{i}(\mathrm{H_2})_{\mathrm{MH}}$ = change in the moles of H_2 in the metal hydride between the i^{th} and i^{th} – 1 measurement.

1. Introduction

The thermodynamic and kinetic properties of TiH_x have been measured at up to 725 °C to test different practical methods for limiting the effects of H_2 permeability and solubility of the sample cell reactor (SCRs) used during hydrogen sorption characterisation of high-temperature metal hydrides (HTMHs). There is renewed interest in using high-temperature metal hydrides (HTMHs) that operate between 600 °C and 800 °C as low-cost, high-density thermal energy storage (TES) materials [1-5] for use with next-generation Concentrating Solar Power (CSP) [6]. However, metal hydrides with high thermodynamic stability have potential use in a wide range of other practical applications related to permanent magnets [7, 8], switchable mirrors [9], powder processing [10-12] and moderator or shielding components for nuclear reactors [13, 14]. A critical step in assessing the potential of any metal hydride candidate is the accurate evaluation of its thermodynamic and kinetic properties utilising pressure-composition-isotherms (PCIs) measurements. However, each data point in a high quality PCI measurement may take hours [15, 16], days [17] or even weeks [18] to collect. Above ≃ 450 °C, the permeability and solubility of hydrogen in the stainless steel (SS) sample cell reactors (SCRs) becomes significant enough to affect the results and suitable methods are required to either limit or account for these effects.

Metal hydrides have a long research history as TES materials[19] and detailed reviews can be found elsewhere [3-5, 20-22]. To properly assess a metal hydride for its potential as a high-temperature TES material requires the accurate

determination of a wide range of properties including thermodynamics, kinetics of hydrogen absorption/desorption, plateau shape and practical hydrogen content. Sieverts-type instruments with SS SCRs are often used for these determinations utilising either step-wise PCI measurements or single-step absorption/desorption measurements. However, the target operating temperature range of future CSP power plants is between 600 and 800 °C and laboratory characterisation of metal hydride properties at these temperatures presents serious challenges due to the hydrogen solubility and permeability of SCRs at high temperature.

Previous research on the properties of metal hydrides at greater than 600 °C have generally used silica or quartz sample cells [23-25], heavy-walled steel sample cells[26, 27] or double-walled steel SCRs [28]. These approaches each have their disadvantages. Silica or quartz sample cells are typically limited to a maximum hydrogen pressure of less than 3 bar and hydrogen diffusion through the reactor walls is still an issue. Heavy-walled steel SCRs have been used at a temperature of up to 707 °C and a maximum hydrogen pressure of $\simeq$ 50 bar[27] while steel SCRs operating between 700 and 1000 °C were used up to a pressure of $\simeq$ 1.2 bar [29]. A pressure equalising double-walled steel SCR capable of operating at 900 °C and hydrogen pressures of more than 650 bar, constructed by Klostermeier and Frank [28], eliminated the effect of hydrogen diffusion but came at the expense of increased experimental complexity and cost with the SCR still being affected by the hydrogen solubility of the steel. This previous work highlights the difficulties faced with accurate lab-scale characterisation of HTMHs that may be promising as TES materials in next-generation CSPs.

For industrial scale applications, steel coated with thin ceramic layers of low hydrogen permeability have been extensively studied for use in conventional power generation, nuclear fission and nuclear fusion applications [30-34]. The hydrogen permeability in ceramics, such as Al_2O_3, TiC, TiN, TiO_2, BN, SiO_2, Cr_2O_3 and SiC, is drastically lower than in metals, Figure 1. Thin ceramic coatings can reduce hydrogen permeability through steel by orders of magnitude and various application techniques can be used, including chemical vapour deposition (CVD), hot-dip aluminisation (HDA), electro-chemical deposition (ECD), packed-bed cementation (PBC) and different types of plasma spraying [34] , to name but a few. However, many of these techniques are not suited to small laboratory-scale equipment and components or are prohibitively expensive. As a result, the development of laboratory-scale methods are required for characterising HTMHs suitable for next generation CSPs.

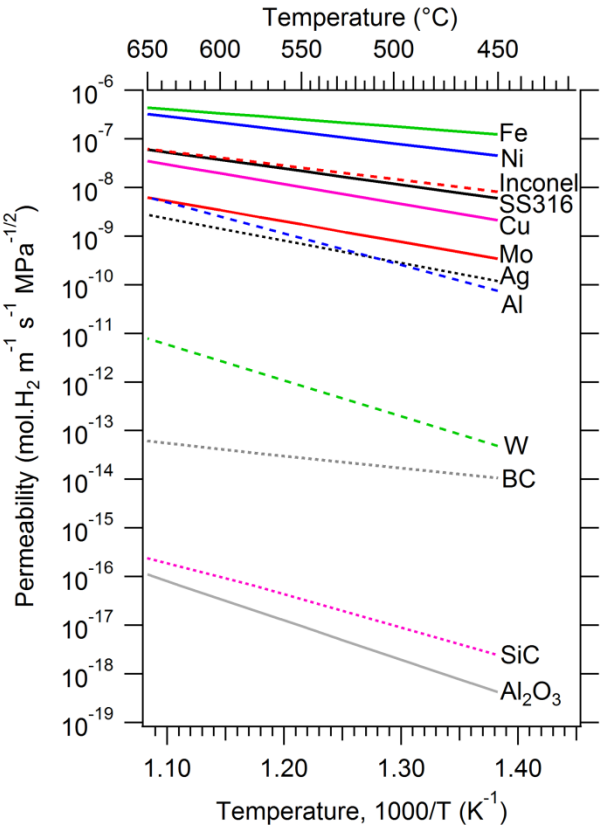

Figure 1. Hydrogen permeability for a number of common materials as a function of temperature [30].

This present investigation is focussed on developing methods for minimising the impact of hydrogen permeability and solubility of SCRs on the high temperature characterisation of metal hydrides. Two different SCRs with reduced hydrogen permeability were constructed and their performance tested by measuring the thermodynamic and kinetic properties of TiH_x at temperatures between 650 and 725 °C. In addition, guidelines and data correction methods were developed for when steel SCRs are the only practical choice for characterising the properties of HTMHs.

2. The Effects of Sample Cell Reactor Hydrogen Permeability and Solubility

A change in the hydrogen gas pressure that SS is exposed to will cause a change in the equilibrium hydrogen concentration, χ, within the steel. The equilibrium hydrogen concentration is a function of the hydrogen solubility, K, and the hydrogen fugacity, f. The solubility is given by $K = K_o \cdot \exp(-\Delta H_s/R \cdot T)$ while the fugacity is given by $f^{½} = (P \cdot Z)^{½}$. Steel exposed to a uniform hydrogen gas pressure has a uniform hydrogen concentration throughout and the amount of hydrogen absorbed by the steel, $n(\mathrm{H_2})_{\chi}^{\mathrm{SS}}$, can be calculated using Equation 1 [35]. However, a SCR is only pressurised with hydrogen internally and the wall of the SCR has a hydrogen concentration gradient, $\Delta\chi$, due to the different pressure each side experiences. Assuming $\Delta\chi$ is linear [36], with negligible hydrogen pressure on the outside of the SCR, the amount of hydrogen absorbed by a SCR, $n(\mathrm{H_2})_{\Delta\chi}^{\mathrm{SCR}}$ in Equation 2, is half that of SS exposed to a uniform hydrogen pressure.

$$n(\mathrm{H_2})_{\chi}^{\mathrm{SS}} = \chi \cdot V^{\mathrm{SS}} = K \cdot f^{\frac{1}{2}} \cdot V^{\mathrm{SS}} = K_o \cdot e^{\left(-\Delta H_s/_{R \cdot T}\right)} \cdot f^{\frac{1}{2}} \cdot V^{\mathrm{SS}} = K_o \cdot e^{\left(-\Delta H_s/_{R \cdot T}\right)} \cdot f^{\frac{1}{2}} \cdot \frac{m^{\mathrm{SS}}}{\rho^{\mathrm{SS}}} \quad \text{Eq 1}$$

$$n(\mathrm{H_2})_{\Delta\chi}^{\mathrm{SCR}} = ½ \cdot K_o \cdot e^{\left(-\Delta H_s/_{R \cdot T}\right)} \cdot f^{\frac{1}{2}} \cdot \frac{m^{\mathrm{SCR}}}{\rho^{\mathrm{SCR}}} = ½ \cdot n(\mathrm{H_2})_{\chi}^{\mathrm{SS}} \quad \text{Eq 2}$$

From this the potential problem of hydrogen solubility in a SS SCR is highlighted in Figure 2. The moles of hydrogen absorbed per 100 g of SS SCR are shown (red curves) as a function of temperature and hydrogen gas pressure calculated using Equation 2 and compared to the moles of hydrogen contained within a metal hydride sample depending on its mass and wt% hydrogen capacity (blue curves). For example, consider a metal hydride sample that weighs 0.5 g and has a hydrogen capacity of 4 wt% (Point A). At a hydrogen pressure of 100 bar and a temperature of 700 °C, a 100 g SS SCR will absorb a quantity of hydrogen (Point B) equivalent to ≃ 14% of that contained in the entire metal hydride sample. This is consistent with the results of Klostermeier [28] who observed that the SS components of their SCR were responsible for between 15 and 40% of the hydrogen consumed in their measurements on sodium hydride, NaH.

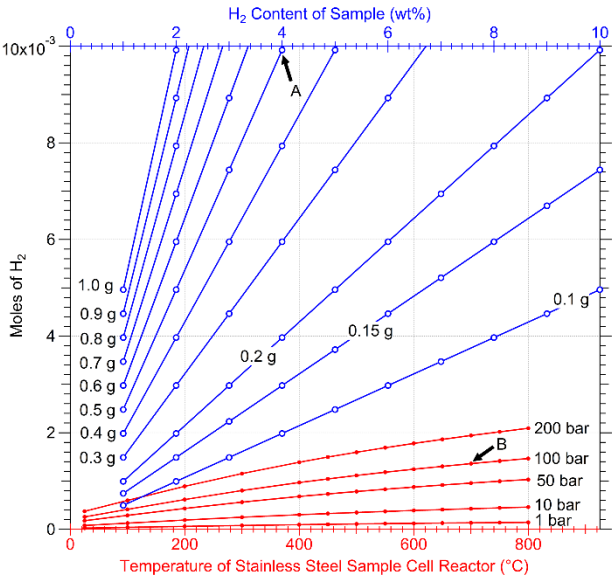

Figure 2. Moles of H_2 absorbed per 100 g of SS as a function of temperature at selected pressures (red) and moles of H_2 contained within a metal hydride as a function of H_2 capacity for selected sample masses (blue).

The hydrogen permeability of a SCR results in a continuous loss hydrogen from the gas phase in a Sieverts-type instrument. Unless accounted for, this decrease would erroneously be attributed to the metal hydride sample in the SCR. Equation 3, derived from San Marchi et al. [35], can be used to calculate the number of moles of hydrogen, $n(\mathrm{H_2})_{\Phi}^{\mathrm{SCR\ calc.}}$, that permeate through a SS flat plate during a given time period:

$$n(\mathrm{H_2})_{\Phi}^{\mathrm{SCR\ calc.}} = SA \cdot J_{\infty} \cdot s = SA \cdot \frac{\Phi}{t} \cdot f^{\frac{1}{2}} \cdot s = \left(\frac{SA}{t}\right)_{\mathrm{eff}} \cdot \Phi \cdot f^{\frac{1}{2}} \cdot s = \left(\frac{SA}{t}\right)_{\mathrm{eff}} \cdot \Phi_o \cdot e^{\left(-H_{\Phi}/R \cdot T\right)} \cdot f^{\frac{1}{2}} \cdot s \qquad \text{Eq 3}$$

As the SCRs used with Sieverts-type instruments are cylindrical and may have complex geometries, the values of the *SA* and *t* variables from Equation 3 are not always known. If the steady state hydrogen loss due to permeation through a SCR can instead be measured, $n(\mathrm{H_2})_{\Phi}^{\mathrm{SCR\ meas.}}$, then Equation 3 can be rearranged so that *SA* and *t* can be replaced by a single variable that is dependent on the geometry of the SCR, $(SA/t)_{\mathrm{eff}}$, Equation 4.

$$\left(\frac{SA}{t}\right)_{\mathrm{eff}} = \frac{n(\mathrm{H_2})_{\Phi}^{\mathrm{SCR\ meas.}}}{\Phi \cdot f^{\frac{1}{2}} \cdot s} \qquad \text{Eq 4}$$

Figure 3 shows the amount of hydrogen lost to permeation over 24 h for a 316L-SS SCR, with $(SA/t)_{\mathrm{eff}}$ = 1, as a function of temperature at selected pressures (red curves) and compares it to the amount of hydrogen contained within a metal hydride depending on the hydrogen capacity and sample mass (blue curves). The duration of 24 h was chosen as a useful compromise between single-step absorption measurements that are often between 6 and 24 h long and PCI measurements along the plateau where individual data points may take as little as 2 h [15] or as much as 24 h to collect [17]. Again, as an example, consider a metal hydride sample of 0.5 g in mass with a hydrogen content of 4 wt% (Point A in Figure 3. A SS SCR at 700 °C and a hydrogen pressure of 25 bar (Point B in Figure 3) would lose ≃ 1.5 times the quantity of hydrogen through permeation than that contained in the metal hydride sample.

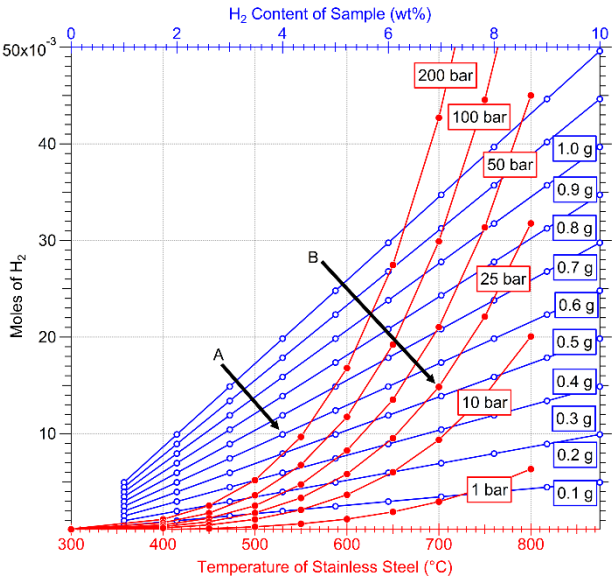

Figure 3. Moles of H_2 lost to permeation through SS, $(SA/t)_{\mathrm{eff}}$ = 1, over 24 h as a function of temperature at selected pressures (red) and moles of H_2 contained within a metal hydride as a function of H_2 capacity for selected sample masses (blue). For context, an 8.0 cm length of SS tubing with a wall thickness of 0.21 cm would have an $(SA/t)_{\mathrm{eff}}$ of 1.01, an internal volume of 4.52 cm³ and a mass of 44.6 g.

3. Experimental Information

3.1 Sieverts-type Instruments for Hydrogen Studies

The Sieverts-type instrument used to measure pressure-composition-isotherms (PCI) of TiH_x and to measure hydrogen leak rates through pure SS SCRs is shown in Figure 4 [37]. Briefly, the pressure was measured using a Rosemount pressure transducer (Model 3051S_T) with an accuracy (±2σ), based on the calibration certificate, of 0.01% of its full scale (150 bar). The reference volume of the Sievert-type instrument was constructed using Swagelok VCR-type sealing fittings while the SCR was constructed using a combination of Swagelok VCR- and tube-type sealing fittings. Depending

on the SCR used, the total internal system volume was between 28 and 50 cm^3. The ambient temperature was measured using either a K-type thermocouple or a 4-wire platinum resistance temperature detector (RTD). The sample temperature measurements were monitored using a K-type thermocouple. The volumetric instruments had a hydrogen sensitivity of between $\simeq 5 \times 10^{-5}$ and $\simeq 10 \times 10^{-5}$ moles, depending on the system volumes. An Anest Iwata ISP 90 oil free scroll vacuum pump, achievable vacuum of ~5×10^{-2} mbar, was used for evacuation of the system.

3.2 Pressure-Composition-Isotherm measurements of TiH_x

Titanium (99.7% trace metals analysis, 2 mm thick sheet, Sigma-Aldrich) was cut into chips (2 mm x 5 mm) but was otherwise used as received. PCI measurements, including kinetic data, were performed using both Al-coated 316L-SS (T = 652.2, 671.8 and 701.4 °C) and α-SiC SCRs (T = 672.6, 689.7 and 724.5 °C). Only the plateau that forms due to the coexistence of the β-Ti and δ-phase is of relevance for CSP and, at 650 °C, occurs for $\simeq 1.04 < H/M < \simeq 1.57$ [38]. The β-Ti phase is a random interstitial alloy of H in the body-centred cubic structure of elemental β-Ti while the δ-phase is a Ti-H with a face-centred cubic structure [38]. Consequently, PCI measurements were generally performed for $\simeq 0.75 < H/M < \simeq 1.64$. The titanium chips, ≃ 1.4 - 2.0 g, were contained within a SS sample vial, 12.7 g, capped with a sintered SS porous filter, 0.5 μm. A SS rod, 9.0 g, and sintered alumina rods were added to reduce the internal 'dead-volume' of the SCR. An initial analysis of the collected kinetic data led to the choice of a 4 hour wait-time for each step on the PCI plateau. The titanium was initially activated by first evacuating it and then loading it under a H_2 pressure of 23 bar at room-temperature. The sample was then heated to 600 °C and began to rapidly absorb hydrogen above 550 °C. Corrections were applied to the PCI data as outlined below.

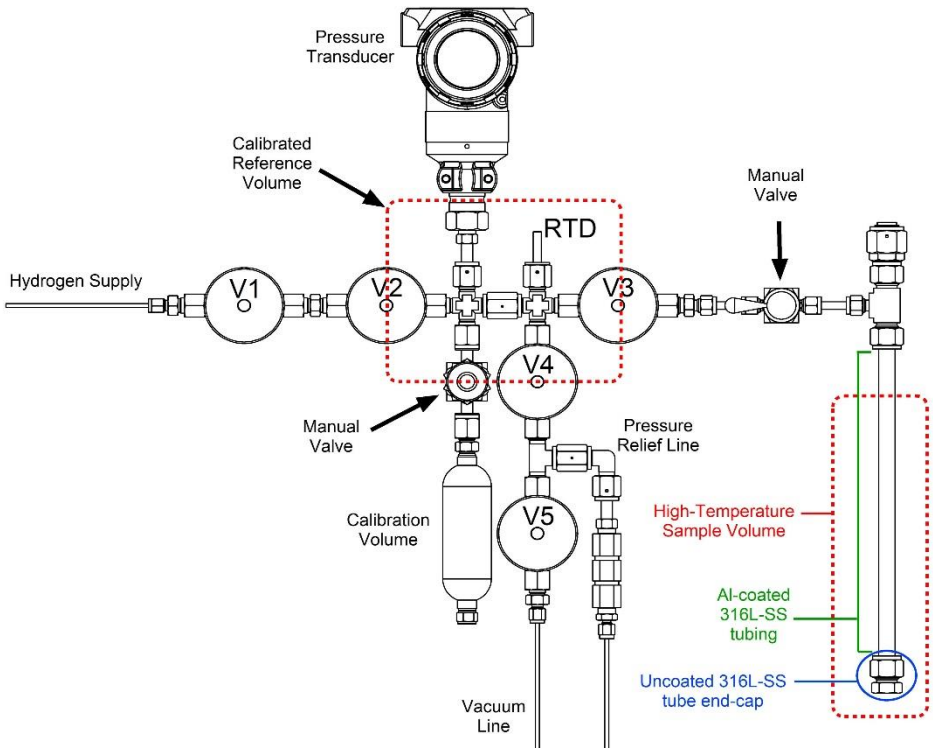

Figure 4: Sieverts-type instrument for high-temperature pressure-composition-isotherm measurements and hydrogen leak tests

3.3 Sample cell reactors

3.3.1 Aluminium-Coated Stainless Steel Sample Cell Reactor

Aluminising is the name used for a number of different techniques that result in a layer of an aluminium-based intermetallic alloy on a steel or nickel-based substrate [39]. The aluminium-coated SCRs used in this study were produced using the commercially available EndurAlizing™ (or Alonizing) process. This is a packed-bed cementation technique where the component to be coated is surrounded by a mixture of blended aluminium powders and heated

to initiate a reaction between the aluminium powder and the steel surface. SCRs were constructed from aluminised 300 mm lengths of ½" 316L SS tubing (OD = 12.7 mm, ID = 8.5 mm, Swagelok), various tube fittings and a valve for sample isolation, Figure 4. Both the internal and external surfaces of the 300 mm lengths of the ½" tubing were Al-coated but the bottom of the tubing was sealed with an uncoated ½" 316L SS end cap fitting. The aluminising process resulted in a surface with higher roughness than the original steel tubing and in order to ensure a gas tight seal, the ends of Al-coated tubing had to be first polished with 1200 grit sandpaper. The uncoated ½" end cap fitting had a steel mass of 36.4 g in contact with hydrogen gas in addition to the mass of the steel sample vial and spacer. Due to the uncoated end cap, the SCR had a $(SA/t)_{eff}$ value of 0.14.

Safety Warning: Please note that the increase in hardness of the intermetallic surface layer relative to uncoated SS means that tubing and tube fittings are used in a manner that has not been certified by the manufacturer and a hazard risk assessment should be performed before replicating this experimental configuration.

3.3.2 α-SiC Sample Cell Reactor

Silicon carbide (α-SiC) thermowell protection tubes (Hexoloy® SA SiC) were purchased from Saint-Gobain, France (specified with grain size < 10 μm and > 98% theoretical density) [40]. The SiC tubes were closed at one end (length of 450 mm, outer diameter (O.D.) of $\simeq$ 16.2 mm, wall thicknesses of $\simeq$ 2.9 mm and inner diameter (I.D.) of $\simeq$ 10.4 mm). The SiC tubes were connected to the volumetric equipment using Swagelok® tube fittings and either graphite or Teflon® ferrules. Burst testing using water at 25 °C was performed according to Australian Standards AS1180.5 (Maximator®, Australia) to establish a safe maximum hydrogen pressure when used as part of a Sieverts-type instrument with further details provided in the supporting information.

Safety Warning: Please note that the manner in which the SiC tubing and tube fittings, used here, are not certified by the manufacturers and a hazard risk assessment should be performed before replicating this experimental configuration. In particular, the potential for high-temperature reactivity between the SiC tubing and metal components, such as sample vials and thermocouple sheaths, should be taken into account [41-43].

3.3.3 316L Stainless Steel Sample Cell Reactor

In order to derive a method to correct sorption measurements of metal hydrides affected by the use of steel SCRs, the Sieverts-type instrument described above was used for performing hydrogen permeability tests of a SCR constructed of 316L SS. The SCR was comprised of ½" 316L SS tubing (OD = 12.7 mm, ID = 8.5 mm, length = 50 mm) ½" 316L SS tube fittings (Swagelok®). The SCRs were connected to the volumetric instrument via ¼" 316L SS tubing (OD = 6.35 mm, ID = 0.15 mm). Hydrogen leak tests were performed at 4 different temperatures (T = 486.3, 506.5, 557.7 and 657.5 °C) and the corresponding $(SA/t)_{eff}$ values were calculated. After the leak test at the highest temperature, a repeat measurement was undertaken at 486 °C to assess the potential impact of oxidation on the hydrogen leak rate. The procedure for measuring the hydrogen leak rate consisted of loading the entire Sieverts instrument, including the SCR, to $\simeq$ 20 bar hydrogen pressure and then raising the temperature to the target temperature where it was held for $\simeq$ 3 days while the decrease in hydrogen pressure was measured. Data was collected at 2 minute intervals.

The coefficients for the hydrogen permeability of 316L SS used in this work were Φ_o = 3.826 × 10^{-4} mol $H_2 \cdot m^{-1} \cdot s^{-1} \cdot MPa^{-1/2}$ and $-H_\Phi$ = 66.102 kJ·mol H [35, 44-51] while the coefficients for permeability were K_o = 2.834 × 10^{-6} mol $H_2 \cdot m^{-3} \cdot MPa^{-1/2}$ and $-\Delta H_s$ = 60.202 kJ·mol H [35]. The temperature dependent density of 316-SS used was ρ^{SS} = -1.881 × $10^{-4} \cdot T^2$ – 2.978 × $10^{-1} \cdot T$ + 7945, where ρ^{SS} has units of $kg \cdot m^{-3}$ and T has units of °C [52]. The derivation of these values from the literature is provided in the supporting information, Table S1.

3.4 Correcting Hydrogen Sorption Measurements for Permeability and Solubility of the Sample Cell Reactor

The explanation and notation for performing hydrogen absorption/desorption measurements using a Sieverts-type instrument are based on that of Blach and Gray [53]. Suppose for the Sieverts-type instrument that we have made two measurements separated in time and define them as the $i^{\text{th}} - 1$ and the i^{th} measurement, respectively. Since the Sieverts-type system is a closed system, the total moles of hydrogen contained within the Sieverts-type system is given by:

$$n^i(\mathrm{H_2})_{\mathrm{gas}} + n^i(\mathrm{H_2})_{\mathrm{MH}} = n^{i-1}(\mathrm{H_2})_{\mathrm{gas}} + n^{i-1}(\mathrm{H_2})_{\mathrm{MH}} \qquad \text{Eq 5}$$

By rearranging Equation 5, we can obtain expressions, Equation 6 and 7, for either the moles of hydrogen in the metal hydride sample present after the i^{th} step, $n^i(\mathrm{H_2})_{\mathrm{MH}}$, or for the change in moles of hydrogen in the metal hydride between the i^{th} and i^{th} -1 measurement, $\Delta n^i(\mathrm{H_2})_{\mathrm{MH}}$.

$$n^i(\mathrm{H_2})_{\mathrm{MH}} = n^{i-1}(\mathrm{H_2})_{\mathrm{gas}} - n^i(\mathrm{H_2})_{\mathrm{gas}} + n^{i-1}(\mathrm{H_2})_{\mathrm{MH}} \qquad \text{Eq 6}$$

$$\Delta n^i(\mathrm{H_2})_{\mathrm{MH}} = n^{i-1}(\mathrm{H_2})_{\mathrm{MH}} - n^i(\mathrm{H_2})_{\mathrm{MH}} = -\left[n^{i-1}(\mathrm{H_2})_{\mathrm{gas}} - n^i(\mathrm{H_2})_{\mathrm{gas}}\right] = -\Delta n^i(\mathrm{H_2})_{\mathrm{gas}} \qquad \text{Eq 7}$$

The $n^i(\mathrm{H_2})_{\mathrm{gas}}$ and $n^{i-1}(\mathrm{H_2})_{\mathrm{gas}}$ terms can readily be adapted for use with either step-wise PCI measurements or single-step kinetic measurements.

For a high-temperature ($T > \simeq 450$ °C) hydrogen absorption/desorption measurement performed using a Sieverts-type instrument on a metal hydride, there are up to three additional contributions to the change in the number of moles of hydrogen in the gas phase. The first contribution is due to the permeability of the SCR and will result in a continuous loss of hydrogen from the gas phase during both absorption and desorption measurements. The second contribution is from any steel within the internal volume of the SCR (i.e. a filter-capped steel sample vial) where all surfaces are exposed to the same hydrogen gas pressure of the Sieverts-type system. The third contribution is due to hydrogen solubility within the SCR. Changes in temperature or internal hydrogen pressure lead to a new hydrogen concentration gradient across the wall of the SCR. To take these additional contributions into account, Equation 7 can be modified to yield Equation 8:

$$\Delta n^i(\mathrm{H_2})_{\mathrm{MH}} = -\Delta n^i(\mathrm{H_2})_{\mathrm{gas}} - \Delta n^i(\mathrm{H_2})_{\Phi}^{\mathrm{SCR\ calc.}} - \Delta n^i(\mathrm{H_2})_{\chi}^{\mathrm{SS}} - \Delta n^i(\mathrm{H_2})_{\Delta\chi}^{\mathrm{SCR}} \qquad \text{Eq 8}$$

Where

$$\Delta n^i(\mathrm{H_2})_{\Phi}^{\mathrm{SCR\ calc.}} = n^{i-1}(\mathrm{H_2})_{\Phi}^{\mathrm{SCR\ calc.}} - n^i(\mathrm{H_2})_{\Phi}^{\mathrm{SCR\ calc.}} \qquad \text{Eq 9}$$

$$\Delta n^i(\mathrm{H_2})_{\chi}^{\mathrm{SS}} = n^{i-1}(\mathrm{H_2})_{\chi}^{\mathrm{SS}} - n^i(\mathrm{H_2})_{\chi}^{\mathrm{SS}} \qquad \text{Eq 10}$$

$$\Delta n^i(\mathrm{H_2})_{\Delta\chi}^{\mathrm{SCR}} = n^{i-1}(\mathrm{H_2})_{\Delta\chi}^{\mathrm{SCR}} - n^i(\mathrm{H_2})_{\Delta\chi}^{\mathrm{SCR}} \qquad \text{Eq 11}$$

The cumulative moles of hydrogen absorbed by the metal hydride, $n^N(\mathrm{H_2})_{\mathrm{MH}}$, after N data measurement steps is then given by Equation 12:

Eq 12

$$n^N(\mathrm{H_2})_{\mathrm{MH}} = \sum_{i=1}^{N} \Delta n^i(\mathrm{H_2})_{\mathrm{MH}}$$

3.5 Corrections for the Hydrogen Permeation through the Sample Cell Reactor

The calculated moles of hydrogen permeated by a SCR using Equation 2 is based on the assumption of constant hydrogen fugacity. In practise, the hydrogen fugacity will change continuously during an absorption/desorption measurement on a metal hydride performed using a Sieverts-type instrument. If kinetic data is collected then minimal errors are introduced due to the small time step between data points and the square root relationship between hydrogen permeability and fugacity. If only the equilibrium pressure for each PCI data point is recorded, the error introduced is still relatively small due to the square root dependency of permeability on fugacity combined with the asymptotic behaviour of metal hydrides as they approach their hydrogen equilibrium pressure. The magnitude of the error introduced by this approximation will depend somewhat on the actual hydrogen equilibrium pressure and the kinetics of hydrogen absorption/desorption from the metal hydride. However, as an example, for PCI desorption curves measured on TiH_x using the Al-coated SCR, the error associated with making the approximation of constant pressure did not exceed ≃ 0.5%. Therefore, the right-hand side of Equation 9 can be expanded to obtain the expression for the moles of hydrogen permeated between two consecutive data points, Equation 13:

$$\Delta n^i(\mathrm{H_2})_{\Phi}^{\mathrm{SCR\ calc.}} = \left(\frac{SA}{t}\right)_{\mathrm{eff}} \cdot \Phi_{\mathrm{o}} \cdot \left[e^{\left(-H_{\Phi}/_{R \cdot T^{i-1}}\right)} \cdot \left(f^{i-1}\right)^{\frac{1}{2}} \cdot s^{i-1} - e^{\left(-H_{\Phi}/_{R \cdot T^{i}}\right)} \cdot \left(f^{i}\right)^{\frac{1}{2}} \cdot s^{i}\right] \qquad \text{Eq 13}$$

The cumulative moles permeated after N data measurement steps, $n^N(\mathrm{H_2})_{\Phi}^{\mathrm{SCR\ calc.}}$, is then given by Eq 14:

Eq 14

$$n^N(\mathrm{H_2})_{\Phi}^{\mathrm{SCR\ calc.}} = \sum_{i=1}^{N} \Delta n^i(\mathrm{H_2})_{\Phi}^{\mathrm{SCR\ calc.}}$$

3.6 Corrections for the Hydrogen Solubility in Steel

Hydrogen solubility in steel can affect experimental data collected using a Sieverts-type instrument in two possible ways. The first is for any steel fully contained within the internal volume of the SCR whose surfaces are all exposed to the same pressure. The second is for the SCR steel wall exposed to a difference in hydrogen pressure. For the first case, the correction method is the same for both absorption and desorption measurements. Assuming the steel mass to be constant, substitution of Equation 1 into Equation 10 yields the change in moles of hydrogen dissolved in steel, $\Delta n^i(\mathrm{H_2})_{\chi}^{\mathrm{SS}}$, between two measurements, Equation 15:

$$\Delta n^i(\mathrm{H_2})_{\chi}^{\mathrm{SS}} = K_{\mathrm{o}} \cdot \left[e^{\left(-\Delta H_s/_{R \cdot T^{i-1}}\right)} \cdot \left(f^{i-1}\right)^{\frac{1}{2}} \cdot \frac{m^{\mathrm{SS}}}{\left(\rho^{i-1}\right)^{\mathrm{SS}}} - e^{\left(-\Delta H_s/_{R \cdot T^{i}}\right)} \cdot \left(f^{i}\right)^{\frac{1}{2}} \cdot \frac{m^{\mathrm{SS}}}{\left(\rho^{i}\right)^{\mathrm{SS}}}\right] \qquad \text{Eq 15}$$

The total correction due to the SS contained within the SCR over N data measurement steps is then given by Equation 16:

Eq 16

$$n^N(\mathrm{H_2})_{\chi}^{\mathrm{SS}} = \sum_{i=1}^{N} \Delta n^i(\mathrm{H_2})_{\chi}^{\mathrm{SS}}$$

Corrections for the latter case, $\Delta n^i(\mathrm{H_2})_{\Delta\chi}^{\mathrm{SCR}}$, are more complicated and differ depending on whether an absorption or desorption measurement are being performed. For an absorption measurement step where the final hydrogen pressure is higher than the initial, the change in moles of hydrogen dissolved in the SCR, Equation 17, is instead obtained by substituting Equation 2 into Equation 10. The cumulative correction is then given by Equation 18.

$$\Delta n^i_{\mathrm{abs.}}(\mathrm{H_2})_{\Delta\chi}^{\mathrm{SCR}} = \tfrac{1}{2} \cdot K_{\mathrm{o}} \cdot \left[e^{\left(-\Delta H_s/_{R \cdot T^{i-1}}\right)} \cdot \left(f^{i-1}\right)^{\frac{1}{2}} \cdot \frac{m^{\mathrm{SCR}}}{\left(\rho^{i-1}\right)^{\mathrm{SCR}}} - e^{\left(-\Delta H_s/_{R \cdot T^{i}}\right)} \cdot \left(f^{i}\right)^{\frac{1}{2}} \cdot \frac{m^{\mathrm{SCR}}}{\left(\rho^{i}\right)^{\mathrm{SCR}}}\right] \qquad \text{Eq 17}$$

Eq 18

$$n_{\text{abs.}}^{N}(\text{H}_2)_{\Delta\chi}^{\text{SCR}} = \sum_{i=1}^{N} \Delta n_{\text{abs.}}^{i}(\text{H}_2)_{\Delta\chi}^{\text{SCR}}$$

However, the hydrogen solubility corrections that need to be applied to desorption measurements depend on the circumstances. For measurements that involve a discontinuous decrease in the hydrogen gas pressure of the system, some of the hydrogen absorbed in the SCR will be released back into the volume of the Sieverts-type instrument. However, unlike the case for absorption measurements, the simple difference between the quantities of hydrogen dissolved by the SCR at the two different pressures cannot be used.

Consider a SCR at an internal hydrogen gas pressure of P_B, Figure 5, with an equilibrium hydrogen concentration gradient, $\Delta\chi$, represented by the line between Point B and C (line BC) and the quantity of hydrogen absorbed by the SCR corresponds to the area bound by Points BCOB (area BCOB). If the internal hydrogen pressure is raised to P_A for an absorption measurement, the new $\Delta\chi$ corresponds to line AC and the hydrogen absorbed by the SCR corresponds to area ABCA.

For a hydrogen desorption measurement where the pressure instead starts at P_A and finishes at P_B, the hydrogen within area BCDB will diffuse through the external surface as it has an equilibrium concentration lower than χ_B. However, the absorbed hydrogen associated with area ABDA has a higher equilibrium concentration than χ_B and time-dependent diffusion equations would be required to determine how much hydrogen is released back into the internal volume of the SCR and how much diffuses through the external surface.

To simplify matters, all hydrogen in area ABDA is assumed to be released back into the internal volume and all hydrogen in area BCDB is lost through the external surface of the SCR. This simplification has a number of advantages. The first is that the ratio of hydrogen contained within area ABDA and area ABCA can be related to the hydrogen equilibrium concentrations at Point A and B. This means that the thickness of the wall is not required and this approach can then be applied to SCRs with complex geometries where the concept of wall thickness is poorly defined. The second advantage is that during continuous measurements where there is a gradual and continuous decrease in hydrogen gas pressure, such as in experiments to determine $(SA/t)_{\text{eff}}$, the quantity of hydrogen released by the SCR back into the internal volume approaches zero as the rate of pressure change approaches zero. This assumption will be valid provided the rate of pressure decrease is slow compared to the rate of hydrogen diffusion within the SS. The generalised equation for the quantity of hydrogen desorbed by the SS SCR into the internal volume, $\Delta n_{\text{des.}}^{i}(\text{H}_2)_{\Delta\chi}^{\text{SCR}}$, during a discontinuous pressure decrease is then given by Equation 19:

Eq 19

$$\Delta n_{\text{des.}}^{i}(\text{H}_2)_{\Delta\chi}^{\text{SCR}} = ½ \cdot K_{\text{o}} \cdot \left[e^{\left(-\Delta H_s / R \cdot T^{i-1}\right)} \cdot \left(f^{i-1}\right)^{\frac{1}{2}} \cdot \frac{m^{\text{SCR}}}{(\rho^{i-1})^{\text{SCR}}} - e^{\left(-\Delta H_s / R \cdot T^{i}\right)} \cdot \left(f^{i}\right)^{\frac{1}{2}} \cdot \frac{m^{\text{SCR}}}{(\rho^{i})^{\text{SCR}}} \right] \cdot \left(1 - \frac{\chi^{i} \cdot \left(V^{i}\right)^{\text{SCR}}}{\chi^{i-1} \cdot (V^{i-1})^{\text{SCR}}} \right)$$

When hydrogen sorption measurements are performed at near-constant temperature, the volume of SS in the SCR can be treated as constant and Equation 19 simplifies to:

Equation 20

$$\Delta n_{\text{des.}}^{i}(\text{H}_2)_{\Delta\chi}^{\text{SCR}} = ½ \cdot \frac{m^{\text{SCR}}}{\rho^{\text{SCR}}} \cdot K_{\text{o}} \cdot \left[e^{\left(-\Delta H_s / R \cdot T^{i-1}\right)} \cdot \left(f^{i-1}\right)^{\frac{1}{2}} - e^{\left(-\Delta H_s / R \cdot T^{i}\right)} \cdot \left(f^{i}\right)^{\frac{1}{2}} \right] \cdot \left(1 - \frac{\chi^{i}}{\chi^{i-1}} \right)$$

For this equation it is recommended to retain the temperature for the i^{th} and i^{th} – 1 measurement in the solubility terms due to the exponential relationship between the two.

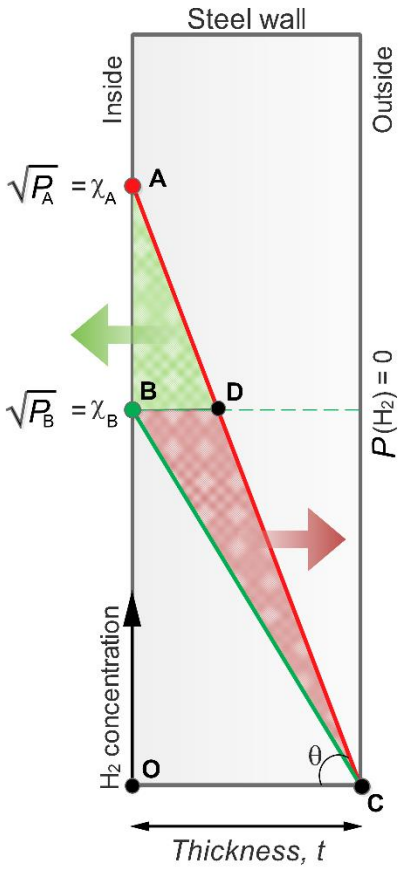

Figure 5. Cross section of a steel wall of a SCR showing the change in the hydrogen concentration gradient that results due to a change in the hydrogen pressure differential experienced by the steel wall.

Determining the $(SA/t)_{eff}$ value for a Sample Cell Reactor

The $(SA/t)_{eff}$ value of an empty SCR can be determined by measuring the decrease in hydrogen pressure over time at temperatures and pressures similar to those to be used for the experiments on the metal hydride sample. This assumes the permeability of the SCR is constant over time and that bulk diffusion of hydrogen through the SS is the rate limiting factor. If the pressure decrease over time is slow compared to the rate of hydrogen diffusion within the steel then we also make the assumption that the hydrogen solubility of the SCR can be ignored. It should be noted that steel held at high temperatures can form an external oxide layer that impacts the total hydrogen permeability.

An initial guess for $(SA/t)_{eff}$ is chosen and Equation 14 is used to calculate the cumulative moles of hydrogen permeated, $n^N(\mathrm{H_2})_{\Phi}^{\mathrm{SCR\ calc.}}$, by the sample cell over time using the experimental conditions. The $(SA/t)_{eff}$ value is then optimised by minimising the residual sum of squares (*RSS*), Equation 21, between the experimentally measured cumulative moles of hydrogen permeated, $n^N(\mathrm{H_2})_{\Phi}^{\mathrm{SCR\ meas.}}$, and the calculated $n^N(\mathrm{H_2})_{\Phi}^{\mathrm{SCR\ calc.}}$.

Eq 21

$$RSS = x \cdot \sum_{N=1} \left[n^N(\mathrm{H_2})_{\Phi}^{\mathrm{SCR\ meas.}} - n^N(\mathrm{H_2})_{\Phi}^{\mathrm{SCR\ calc.}} \right]^2$$

For the data presented in this paper the Generalized Reduced Gradient (GRG) Nonlinear algorithm within the *Solver* add-in for *Microsoft Excel* was used to determine optimised $(SA/_t)_{eff}$ values. A scaling factor, x, is included in Equation 21 and, for this work, an arbitrary value of 1×10^{12} was used to ensure the typical magnitudes of the *RSS* values were large relative to the convergence criterion within *Solver*.

4. Results and Discussion

4.1 Pressure-Composition-Isotherms of TiH_x

The six hydrogen desorption PCI measurements performed on TiH_x between 652 °C and 725 °C are shown in Figure 6(a). The PCI desorption curve performed at 672 °C using the Al-coated SS SCR has been excluded for clarity. The observed plateaux had a width of ≃0.5 H/M that decreased with increasing temperature [29, 38, 54] and was consistent with plateau widths observed in the literature [27, 38]. In contrast, the start of the $\beta + \delta$ plateaux occurred at consistently lower values of hydrogen content than that derived from the literature. For example, at 690 °C the start of the plateau was at H/M = 0.976 compared to a literature interpolated value of 1.076 at this temperature [38]. The PCI desorption curves obtained for TiH_x also showed that each plateau had a very slight slope with an average value of 0.373 $(H/M)^{-1}$ for data collected using the α-SiC SCR (T = 672.6, 689.7 and 724.5 °C) and an average value of 0.489 for data collected with the Al-coated SS SCR (T = 652.2, 671.8 and 701.4 °C). The change in the start position of the plateau can be explained by the modest purity of the titanium used in this study, 99.7% trace metals basis, whereby interstitial nitrogen, oxygen and metal impurities shift the equilibrium to lower hydrogen contents [54, 55]. The effect of metal impurities on the location of the start of the plateau can be particularly pronounced where, for example, hydrogen absorption measurements on the Ti-6Al-4V alloy (5.9 wt% Al, 4.0 wt% V, 0.35 wt% other impurities, 89.75 wt% Ti) at 700 °C showed a decrease of the $\beta + \delta$ plateau onset to H/M ≃ 0.70 compared to a value of H/M ≃ 1.02 for their pure titanium sample [56]. The sloping plateaux can also potentially be explained by the modest purity of the titanium[55, 57] but the potential influence of hydrogen absorption/desorption kinetics[15, 58-60] should also be considered.

However, the higher plateaux slopes observed when using the Al-coated 316L-SS SCR suggests that even the low rate of hydrogen loss from this SCR exceeded the rate of H_2 released as TiH_x approached its equilibrium pressure. This was confirmed by comparing the PCI desorption curves at ≃ 672 °C obtained using both the α-SiC SCR and the Al-coated SCR, Figure 6(b), and implies that, during PCI measurements, even a small rate of hydrogen loss from the SCR due to permeability can impact the measured plateau slopes and, as shown below, the derived thermodynamics. While the plateau slopes observed in PCI measurements of TiH_x performed using the α-SiC SCRs could most likely be explained by the purity of the titanium, the potential influence of hydrogen absorption/desorption kinetics [15, 58-60] should also be considered. A comparison of the absorption and desorption plateau pressures obtained at 652 °C, Figure 6(b), showed an average pressure difference of less than 0.07 bar. This corresponded to an average hysteresis value, $\ln(P_{abs}/P_{des})$, of just 0.044 for $1.00 \leq H/M \leq 1.35$. Such low hysteresis would not be observed if the sample exhibited slow kinetics relative to the equilibration time used for the PCI steps. This confirmed that the plateau slopes observed during PCI desorption measurements of TiH_x obtained using an α-SiC SCR were a result of the titanium purity and not an artefact of the SCR.

The PCI data for the van't Hoff plot collected using both the α-SiC and Al-coated SS SCRs, Figure 6(c), used the fugacity corresponding to the midpoint of the $\beta + \delta$ plateaux (at H/M = 1.25). This yielded thermodynamic desorption values of ΔH_{des} = 164.4 ± 1.8 kJ/mol·H_2 and ΔS_{des} = 181.6 ± 1.8 J/mol·H_2·K (6 measurement temperatures for 652.2 °C ≤ T ≤ 724.5 °C; R^2 = 0.9996; quoted uncertainty values correspond to 1 standard deviation in coefficients of the linear fit). These values are comparable to those reported in the literature for the enthalpy of desorption, 162.6 kJ/mol·H_2 ≤ ΔH_{des} ≤ 167.9 kJ/mol·H_2 [27, 29, 38, 61], and the entropy of desorption, 177.1 J/mol·H_2·K ≤ ΔS_{des} ≤ 183.2 J/mol·H_2·K [27, 29, 38, 61]. A more comprehensive comparison of the thermodynamic quantities available in the literature are given in the supporting information, Table S2. As inferred by the slight differences in the plateau slopes observed between data collected with the α-SiC and the Al-coated SS SCR, the enthalpy and entropy values derived for each type of SCR differ (ΔH_{des} = 166.8 ± 2.6 kJ/mol·H_2 and 161.3 ± 1.7 kJ/mol·H_2, respectively while ΔS_{des} = 184.0 ± 2.7 J/mol·H_2·K and 178.3 ± 1.8 J/mol·H_2·K, respectively). This shows that the hydrogen permeability of a SS SCR can have small but discernible effects on the thermodynamic properties of metal hydrides derived from PCI measurements. However, it may be feasible that kinetic expressions used for modelling absorption and desorption of hydrogen from

metal hydrides[62] could be extended to make estimates of the actual hydrogen equilibrium pressure while taking into account the rate of hydrogen permeated through the SS components of a SCR.

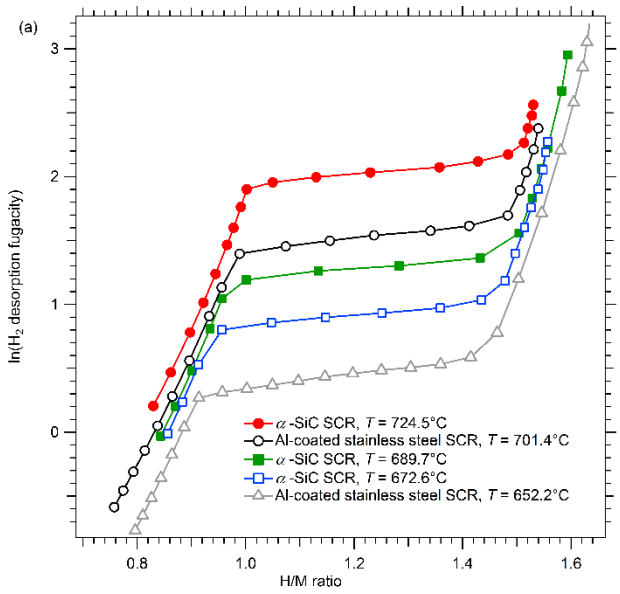

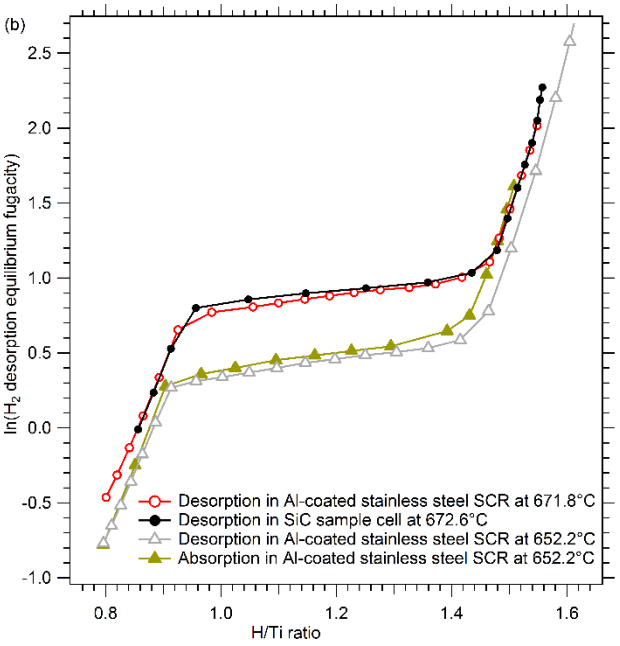

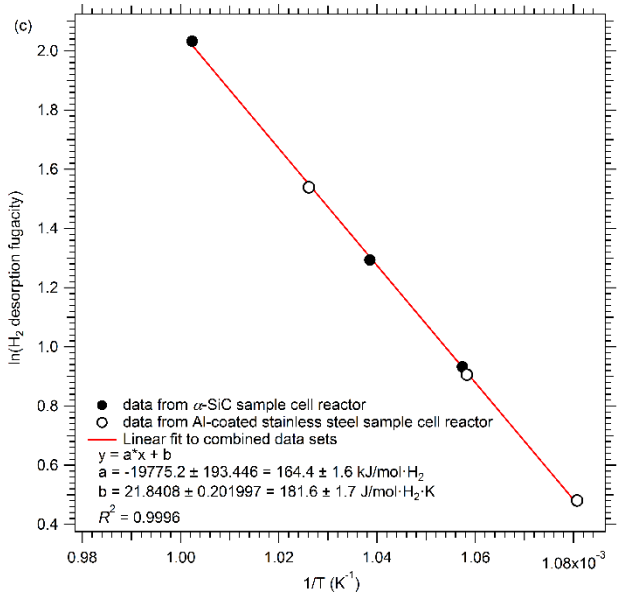

Figure 6. (a) Hydrogen desorption pressure-composition-isotherms for TiH_x at various temperatures; (b) TiH_x desorption PCI curves collected using an α-SiC SCR at 672.6 °C and an Al-coated SS SCR at 671.8 °C and the desorption/absorption PCI curves collected using an Al-coated SS SCR at 652.2 °C; (c) The van't Hoff plot corresponding to a hydrogen-to-metal (H/M) ratio of 1.25.

Careful consideration must be given to the kinetics of hydrogen absorption and desorption in order to obtain accurate metal hydride thermodynamics from PCI measurements [15, 58-60]. Insufficient wait times during desorption PCI measurements will lead to an underestimation of enthalpy and entropy while insufficient wait times during absorption PCI measurements will overestimate enthalpy and entropy. This is particularly problematic for HTMHs where their large enthalpies of desorption/absorption produce self-induced temperature changes via the large aliquot effect[58, 59] and long wait-times are required for the sample to return to thermal equilibrium. As an example, the PCI curve of TiH_x obtained at 689.7 °C and the desorption step between two points on the plateau, Figure 6(a), would induce a temperature decrease of ≃393 °C for a thermally isolated sample (based on m(Ti) = 1.403 g, $n(H_2)_{des}$ = 2.193x10^{-3}, ΔH_{des} = 166.7 kJ/mol·H_2 at H/M = 1.35, $C_p(Ti)_{@690\,°C} \simeq C_p(TiH_x)_{@690\,°C}$ = 31.73 J/mol·K [63]. This highlights the conflict between the high enthalpy of hydrogen absorption/desorption of HTMHs that demand longer PCI step-times against the need to reduce the PCI step-times to minimise the almost certain accumulation of errors associated with the difficulty in choosing appropriate hydrogen permeability coefficients employed in correcting data collected using steel SCRs.

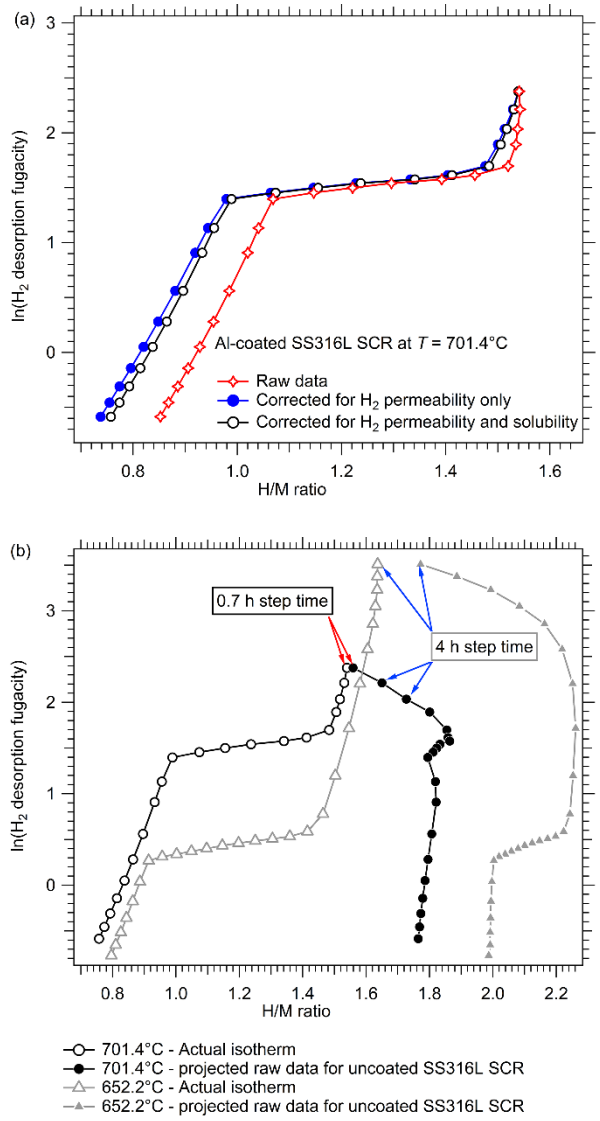

Figure 7. Hydrogen desorption pressure-composition-isotherms (PCI) for TiH_x performed using the Al-coated 316L-SS SCR showing: (a) The raw data as-collected at 701 °C, the raw data corrected for H_2 permeability of the SCR and the raw data corrected for both hydrogen permeability and solubility of the SCR; (b) The PCI curves at 652 °C and 701 °C expected for a 316L-SS SCR that is fully Al-coated and not affected by hydrogen permeability or solubility and the corresponding PCI curves expected for an identical but uncoated 316L-SS SCR.

The raw PCI data collected at 701 °C using the Al-coated 316L-SS SCR is shown in Figure 7(a) in conjunction with the PCI curve corrected for only hydrogen permeability (SA/t = 0.14) and the PCI curve corrected for both hydrogen permeability (SA/t = 0.14) and hydrogen solubility (m(SS) = 58.1 g). This reveals that, for this experimental configuration, there is only a modest effect on the H/M value of the final desorption point. The final raw data desorption point moves from H/M = 0.853 in the raw data to H/M = 0.757 for the fully corrected data and the correction for hydrogen solubility has only a minor influence. While the effect on the PCI data collected using the Al-coated 316L-SS SCR is modest, Figure 7(b) shows the PCI curves to be expected at 701 °C and 652 °C for the same 316L-SS SCR without the Al-coating and a SA/t value of 1.329. In this case, the shape of the PCI desorption curves to be expected for raw data are severely distorted and desorption at high pressures actually results in an increase in the H/M value, instead of the expected decrease. It should be noted that errors in the volume calibrations of the Sieverts-type instrument can also result in PCI curves that show similar behaviour [64]. Figure 7(b) also highlights the importance of choosing a PCI step-time that is appropriate for the position on the desorption curve and the corresponding desorption kinetics. A step-time of 0.7 h (indicated by red arrows) introduces relatively little error for an uncoated 316L-SS SCR whereas a step-time of 4 h (indicated by blue arrows) introduces substantial error. While step-times of 1 h or less may be suitable for PCI data points collected above or below the plateau, for data points located on the plateau, the hydrogen desorption kinetics dictate step-times of several hours or more.

4.2 Results of $(SA/t)_{eff}$ Determination for a Stainless Steel Sample Cell Reactor

To derive a correction method for hydrogen sorption experiments performed on metal hydrides using SS SCRs at temperatures above 450 °C, hydrogen leak tests were performed and the measured cumulative moles of hydrogen lost from the Sieverts-type instrument are shown in Figure 8(a). The red curves in Figure 8 correspond to the optimised $(SA/t)_{eff}$ values that minimised the *RSS* between the observed moles of hydrogen lost and the calculated moles of hydrogen lost over the whole measurement time, Table S3. It should be noted that $(SA/t)_{eff}$ values obtained for data collected for 24 h or less were inconsistent. This can probably be attributed to some combination of quantity of hydrogen lost during this period compared to the sensitivity of the Sieverts-type instrument, the kinetics of establishing steady state hydrogen permeation and the influence that the possible formation of SS oxides may have. The differences between the calculated and observed data are shown in Figure 8 and reveal that the observed hydrogen losses at 486 °C and 507 °C are well represented by the optimised $(SA/t)_{eff}$ values that are $\simeq$ 0.72. This is in broad agreement with a crude value of 0.76 calculated based on the different wall thicknesses for various sections of the SCR. In contrast, the differences between the calculated and observed curves showed systematic deviations for the measurements at 558 and 658 °C, respectively. The optimised $(SA/t)_{eff}$ values for these two temperatures initially underestimated and then overestimated the cumulative moles of hydrogen permeated. To better reproduce the observed number of moles permeated, the $(SA/t)_{eff}$ value would need to be higher and lower at the beginning and end of the measurement time, respectively. Since the physical geometry of the SCR is fixed, the variation in $(SA/t)_{eff}$ corresponds to a change in the apparent permeability of hydrogen during the course of the measurements at 558 and 658 °C respectively.

Surface conditions have a marked effect on experimental measurements of hydrogen permeability[31, 35] and the results observed here can be explained by the growth of an oxide layer on the external surface of the SS SCR. As the temperature increases, oxidation of the external surface SS SCR produces a barrier that hinders the diffusion of hydrogen from the surface and results in a reduction in the apparent permeability of hydrogen. An oxidised internal steel surface exposed to hydrogen pressure can reduce the rate of hydrogen diffusion by orders of magnitude, but an oxidised external steel surface is substantially less effective as evolution of the dissolved hydrogen can damage the oxide coating [31]. This is consistent with the results presented here for the measurements at the two highest temperatures when optimised $(SA/t)_{eff}$ values, derived for consecutive 24 h time frames, showed a slight decrease with measurement time. This is also consistent with the observation that the $(SA/t)_{eff}$ value for the repeat measurement at 486 °C is slightly higher than the preceding $(SA/t)_{eff}$ value for 658 °C: The repeat measurement at 486 °C had the greatest pressure increase at the beginning of the measurement when loading a fresh supply of hydrogen and was more likely to damage the external oxide layer.

The first 5 hours of data collected during the repeat measurement at 486 °C highlights an additional issue related to the kinetics of absorption by the SCR as seen in Figure 9. The red curve corresponds to an extrapolation of the calculated number of hydrogen moles lost using the $(SA/t)_{eff}$ value that was fitted to the observed data between 24 and 328 h. This shows that when the hydrogen pressure was increased from ≃ 6.3 bar to ≃ 21.5 bar, the 120.7 g SS SCR took between 3 and 4 h for its hydrogen concentration to reach equilibrium and for the permeability to reach a steady state process. While the time required to achieve steady state permeability will vary depending on hydrogen pressure change and the mass of the SCR, it helps to provide guidance in choosing suitable step-times so that PCI measurements are not affected by the kinetics of hydrogen dissolution in the steel SCR.

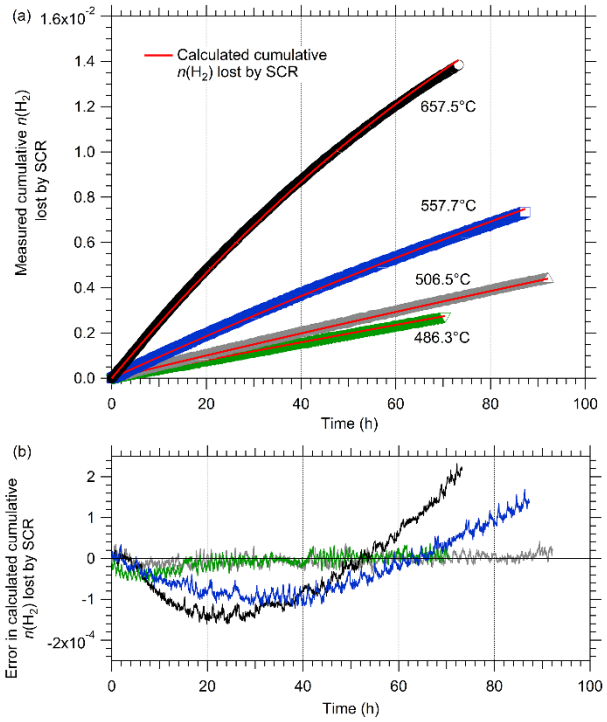

Figure 8. (a) A plot of the measured cumulative moles of hydrogen lost from a 316L-SS SCR vs time at various temperatures (open coloured symbols) and the calculated moles of hydrogen lost vs time for optimised $(SA/t)_{eff}$ values. (b) The difference between the measured moles of hydrogen and the calculated moles of hydrogen lost at various temperatures for optimised $(SA/t)_{eff}$ values.

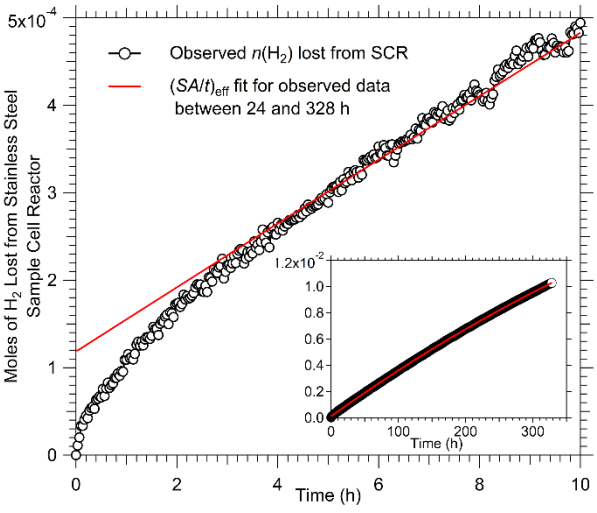

Figure 9. The moles of hydrogen permeated at 486 °C by a 316L-SS SCR during the first 5 h of measurement (open circles) and the $(SA/t)_{eff}$ value corresponding to steady-state permeation that occurred between 24 and 328 h of measurement time (red line). Insert: The moles of hydrogen permeated by the SCR over the entire measurement time.

4.3 Sensitivity Analysis of the Impact of Hydrogen Permeability of the SCR on PCI Measurements

A sensitivity analysis was performed to compare the effect of different experimental factors on the quantity of hydrogen permeated by a 316L-SS SCR compared to the quantity of hydrogen quantity in a sample, Figure 10. The baseline scenario consisted of a hydride sample mass of 1 g with a hydrogen content of 5 wt%. The equilibrium pressure was assumed to be 10 bar at 650 °C and the 316L-SS SCR was assumed to have a $(SA/t)_{eff}$ value of 1.0. Lastly, the PCI curve was assumed to be comprised of 20 steps (data points) with a duration of 3 hours for each step. Under this baseline scenario, the amount of hydrogen permeated by the 316L-SS SCR is as large as ≃ 61 % of the hydrogen quantity in the sample. If a SCR with reduced hydrogen permeability is not available then the impact of hydrogen permeation by a SS SCR can be reduced to acceptable levels by a judicious choice of sample mass, total number of PCI steps and step-time for non-plateau PCI points. For example, if the sample mass is doubled to 2.0 g, the number of 3 h steps along the plateau reduced to 10 and the number of 1 h steps before and after the plateau reduced to 3 each, then the amount of hydrogen permeated by the 316L-SS SCR compared to the hydrogen quantity in the sample is reduced to ≃ 18 %. As a comparison, the hydrogen permeability correction for the desorption curve in Figure 7(a) was 14.5% of the hydrogen quantity released by the sample. Since manipulation of the number of PCI points and their step-times requires a high degree of sample knowledge and instrument control, the simplest approach is to increase the sample mass. As an aid to choosing appropriate experimental parameters to minimise the impact of high-temperature hydrogen permeability of the SCR on hydrogen sorption measurements, an Excel spreadsheet has been created and included in the supporting information.

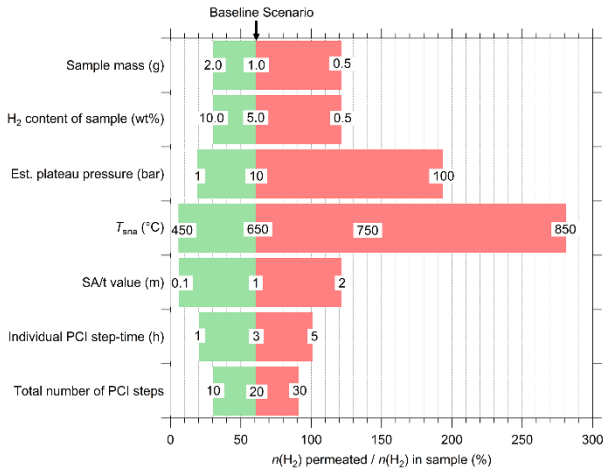

Figure 10. Sensitivity analysis to experimental parameters of the moles of hydrogen permeated through a SS SCR compared to the moles of hydrogen contained within the metal hydride sample being measured. The baseline case parameters are: sample mass = 1.0 g, H_2 content of sample = 5.0 wt%, estimated plateau pressure = 10 bar, non-ambient sample temperature = 650 °C, $(SA/t)_{eff}$ value = 1.0 m, step-time for individual PCI data points = 3 h, total number of PCI steps = 20. Red bars indicate an increase over the baseline scenario in the relative number of hydrogen moles permeated through a 316L-SS SCR. Green bars indicate a decrease.

4.4 Recommended Guidelines for Characterising High-Temperature Metal Hydrides

Ideally, the hydrogen sorption properties of HTMHs would be measured using SCRs unaffected by hydrogen permeability and solubility. The following guidelines have been developed to aid the choice of experimental conditions that minimises the impact of using steel SCRs when characterising high-temperature metal hydrides:

1) If possible, choose a SCR constructed from a material with a low hydrogen solubility and a low hydrogen permeability, e.g. α-SiC.
2) Determine the $(SA/t)_{eff}$ for the empty SS SCR so that it can be used to correct subsequent experimental data. The highest temperature required for experiments with the metal hydride sample should be used since the SCR oxidation will be greatest and the decrease in $(SA/t)_{eff}$ will be the highest. A high starting pressure increases the rate of permeation and allows for more obvious pressure drops. It is recommended that this

measurement should be as long as practically possible but the minimum duration will depend on the specifications of the Sievert's-type instrument used in addition to the temperature and initial hydrogen pressure used for the measurement. For a Sieverts-type instrument similar to that used in the work presented here, three days is recommended. Also, note that the oxidation layer on steel will change over time so $(SA/t)_{eff}$ should be regularly checked.

3) Use as much sample mass as practical for hydrogen absorption/desorption measurements.
4) Minimise the duration of the hydrogen absorption/desorption measurements as much as possible while allowing sufficient time for the sample's hydrogen absorption/desorption kinetics.
5) Choose practically achievable experimental parameters to reduce the predicted hydrogen moles permeated by the SCR compared to moles of hydrogen contained in the sample. Experience within our laboratory suggests that the "permeation-to-sample" ratio should not exceed about 30% and that a value of less than 20% is preferable.

Depending on the characteristics of the Sieverts-type instrument, the metal hydride mass and the absorption/desorption kinetics, the PCI curves required to produce high quality van't Hoff plots can usually take between 1 and 4 weeks to collect. As a result, initial time spent characterising an initial "fast" PCI measurement on the metal hydride can provide information that can be used to choose experimental parameters for subsequent PCI measurements that minimises the impact of the hydrogen permeability of the SCR. It is recommended that this initial "fast" PCI measurement at the midpoint of the intended experimental temperature range is performed on the metal hydride using PCI step-times of $\simeq$ 2 h. This also provides information on the kinetics of hydrogen absorption/desorption at different points along the PCI curve.

5. Conclusion

The accurate characterisation of HTMH properties is a crucial requirement for determining their potential in practical applications. Our focus is on CSP heat storage but, as an example, the experimental techniques described here are also relevant high-temperature rare-earth hydrides that show promise in applications related to permanent magnets and switchable mirrors where fundamental knowledge about their thermodynamic properties is required. In this work we show the impact of the hydrogen permeability and solubility of SS SCRs commonly used with Sieverts-type instruments to characterise metal hydrides at 450 °C and above. Two SCRs with reduced hydrogen permeability and solubility were constructed from commercially available α-SiC tubing and aluminium-coated 316L SS tubing, respectively, and the thermodynamics of TiH_x were then assessed as a measure of their effectiveness. In particular, the α-SiC SCR used has lower hydrogen permeability and solubility than SCRs constructed of other materials and can potentially be used at higher temperatures and hydrogen pressures. However, the brittle nature of ceramics means that, compared to a SS SCR, α-SiC incurs additional technical and safety challenges and a thorough characterisation of its performance limits is required. For Sieverts-type instruments used to characterise metal hydrides where steel is the only practical choice for the SCR, we have developed quantitative methods to correct data and minimise the impact of the SCR hydrogen permeability and solubility. The work presented here is the first time that the impact the SCR hydrogen permeability and solubility has on the data collected has been quantified and a generalised approach developed to account for it. We believe that the methods developed in this work are a significant step for accurately characterising the properties of HTMHs suitable for applications such as heat storage for concentrating solar power.

Acknowledgements

The authors acknowledge the financial support of the Australian Research Council (ARC) for ARC Linkage grant LP120101848 and LP150100730 while ARC LIEF grant LE0989180 enabled the hydrogen sorption measurements to be undertaken. The authors also acknowledge the facilities and technical assistance of the Microscopy & Microanalysis Facility of the John de Laeter Centre at Curtin University. DAS and MP acknowledge their Curtin University Early Career Research Fellowships for financial support. MP also acknowledges his Australian Research Council (ARC) Future Fellowship FT160100303 for financial support.

References

[1] D.N. Harries, M. Paskevicius, D.A. Sheppard, T. Price, C.E. Buckley, Concentrating solar thermal with storage using metal hydrides for low cost dispatchable energy, Proceedings of the IEEE, 100 (2012) 539-549.
[2] M. Fellet, C.E. Buckley, M. Paskevicius, D.A. Sheppard, Research on metal hydrides revived for next-generation solutions to renewable energy storage, MRS Bulletin, 38 (2013) 1012-1013.
[3] D.A. Sheppard, M. Paskevicius, T.D. Humphries, M. Felderhoff, G. Capurso, J. Bellosta von Colbe, M. Dornheim, T. Klassen, P.A. Ward, J.A. Teprovich, C. Corgnale, R. Zidan, D.M. Grant, C.E. Buckley, Metal hydrides for concentrating solar thermal power energy storage, Applied Physics A, 122 (2016) 395.
[4] D.A. Sheppard, T.D. Humphries, C.E. Buckley, Sodium-based hydrides for thermal energy applications, Applied Physics A, 122 (2016) 406.
[5] P.A. Ward, C. Corgnale, J.A. Teprovich, T. Motyka, B. Hardy, D. Sheppard, C. Buckley, R. Zidan, Technical challenges and future direction for high-efficiency metal hydride thermal energy storage systems, Applied Physics A, 122 (2016) 462.
[6] U.D.o. Energy, SunShot Vision Study, Chapter 5: Concentrating Solar Power: Technologies, Cost, and Performance, in, 2012, pp. 97-123.
[7] K. Binnemans, P.T. Jones, B. Blanpain, T. Van Gerven, Y. Yang, A. Walton, M. Buchert, Recycling of rare earths: a critical review, Journal of Cleaner Production, 51 (2013) 1-22.
[8] R.S. Mottram, B. Davis, V.A. Yartys, I.R. Harris, The use of metal hydride powder blending in the production of NdFeB-type magnets, International Journal of Hydrogen Energy, 26 (2001) 441–448.
[9] J.N. Huiberts, R. Griessen, J.H. Rector, R.J. Wijngaarden, J.P. Dekker, D.G. de Groot, N.J. Koeman, Yttrium and lanthanum hydride films with switchable optical properties, Nature, 380 (1996) 231.
[10] O.N. Senkov, F.H. Froes, Thermohydrogen processing of titanium alloys, International Journal of Hydrogen Energy, 24 (1999) 565-576.
[11] I.M. Robertson, G.B. Schaffer, Review of densification of titanium based powder systems in press and sinter processing, Powder Metallurgy, 53 (2013) 146-162.
[12] C.L. Huffine, Fabrication of Hydrides, in: W.M. Mueller, J.P. Blackledge, G.G. Libowitz (Eds.) Metal Hydrides, Academic Press, New York, 1968, pp. 675-747.
[13] W.M. Mueller, Hydrides in Nuclear Reactor Applications, in: W.M. Mueller, J.P. Blackledge, G.G. Libowitz (Eds.) Metal Hydrides, Academic Press, New York, 1968, pp. 22-50.
[14] M.M.H. Bhuiya, A. Kumar, K.J. Kim, Metal hydrides in engineering systems, processes, and devices: A review of non-storage applications, International Journal of Hydrogen Energy, 40 (2015) 2231-2247.
[15] D.A. Sheppard, M. Paskevicius, C.E. Buckley, Thermodynamics of Hydrogen Desorption from $NaMgH_3$ and Its Application As a Solar Heat Storage Medium, Chemistry of Materials, 23 (2011) 4298-4300.
[16] D.A. Sheppard, C. Corgnale, B. Hardy, T. Motyka, R. Zidan, M. Paskevicius, C.E. Buckley, Hydriding characteristics of $NaMgH_2F$ with preliminary technical and cost evaluation of magnesium-based metal hydride materials for concentrating solar power thermal storage, RSC Advances, 4 (2014) 26552-26562.
[17] B. Huang, K. Yvon, P. Fischer, Synthesis, structure and thermal stability of $Yb_4Mg_4Fe_3H_{22}$, Journal of Alloys and Compounds, 197 (1993) 65-68.
[18] J. Graetz, Y. Lee, J.J. Reilly, S. Park, T. Vogt, Structures and thermodynamics of the mixed alkali alanates, Physical Review B (Condensed Matter and Materials Physics), 71 (2005) 184115-184117.
[19] G.G. Libowitz, Metal hydrides for thermal energy storage, in: Proceedings of the Intersociety Energy Conversion Engineering Conference, San Francisco, California USA, 1974, pp. 322-325.
[20] A. Reiser, B. Bogdanović, K. Schlichte, The application of Mg-based metal-hydrides as heat energy storage systems, International Journal of Hydrogen Energy, 25 (2000) 425-430.
[21] M. Felderhoff, B. Bogdanović, High Temperature Metal Hydrides as Heat Storage Materials for Solar and Related Applications, International Journal of Molecular Sciences, 10 (2009) 325-344.
[22] Qiwen Lai, M. Paskevicius, D.A. Sheppard, C.E. Buckley, A.W. Thornton, M.R. Hill, Q. Gu, J. Mao, Z. Huang, H.K. Liu, Z. Guo, A. Banerjee, S. Chakraborty, R. Ahuja, K.-F. Aguey-Zinsou, Hydrogen Storage Materials for Mobile and Stationary Applications: Current State of the Art, ChemSusChem, 8 (2015) 2789-2825.
[23] G.G. Libowitz, A Pressure-Composition-Temperature Study of the Zirconium-Hydrogen System at High Hydrogen Contents, Journal Of Nuclear Materials, 5 (1962) 228-233.
[24] H.F. Franzen, A.S. Khan, D.T. Peterson, Equilibrium Hydrogen Pressures in the Barium-Hydrogen System, Journal of the Less-Common Metals, 65 (1979) 111 - 116.
[25] A. Mascaro, C. Toffolon-Masclet, C. Raepsaet, J.-M. Joubert, Experimental study and thermodynamic assessment of the erbium–hydrogen binary system, Calphad, 41 (2013) 50-59.

[26] P.S. Rudman, J.J. Reilly, R.H. Wiswall, Hydrogen Absorption in Ti_3Al, Berichte der Bunsengesellschaft für physikalische Chemie, 81 (1977) 76-80.
[27] M. Arita, K. Shimizu, Y. Ichinose, Thermodynamics of the Ti-H System, Metallurgical Transactions A, 13 (1982) 1329-1336.
[28] W. Klostermeier, E.U. Franck, Liquid Mixtures of Sodium and Sodium Hydride at High Pressures and Temperatures, Berichte der Bunsengesellschaft für physikalische Chemie, 86 (1982) 606-612.
[29] R.L. Beck, Research and development of metal hydrides, in, Denver University, Denver Research Inst., Summary Report for October 1, 1958-September 30, 1960. No. LAR-10, pp. 1-93.
[30] R.A. Causey, R.A. Karnesky, C. San Marchi, Tritium Barriers and Tritium Diffusion in Fusion Reactors, in: R.J.M. Konings (Ed.) Comprehensive Nuclear Materials, Elsevier, Oxford, 2012, pp. 511-549.
[31] P.S. Flint, The diffusion of hydrogen through materials of construction, in, Knolls Atomic Power Laboratory, 1951, pp. 1-104.
[32] G.W. Hollenberg, E.P. Simonen, G. Kalinin, A. Terlain, Tritium/hydrogen barrier development, Fusion Engineering and Design, 28 (1995) 190-208.
[33] A. Perujo, K.S. Forcey, Tritium permeation barriers for fusion technology, Fusion Engineering and Design, 28 (1995) 252-257.
[34] X. Xiang, X. Wang, G. Zhang, T. Tang, X. Lai, Preparation technique and alloying effect of aluminide coatings as tritium permeation barriers: A review, International Journal of Hydrogen Energy, 40 (2015) 3697-3707.
[35] C. San Marchi, B.P. Somerday, S.L. Robinson, Permeability, solubility and diffusivity of hydrogen isotopes in stainless steels at high gas pressures, International Journal of Hydrogen Energy, 32 (2007) 100-116.
[36] N.A. Al-Mufachi, S. Nayebossadri, J.D. Speight, W. Bujalski, R. Steinberger-Wilckens, D. Book, Effects of thin film Pd deposition on the hydrogen permeability of $Pd_{60}Cu_{40}$ wt% alloy membranes, Journal of Membrane Science, 493 (2015) 580-588.
[37] M. Paskevicius, D.A. Sheppard, C.E. Buckley, Thermodynamic Changes in Mechanochemically Synthesized Magnesium Hydride Nanoparticles, Journal of the American Chemical Society, 132 (2010) 5077-5083.
[38] F.D. Manchester, A. San-Martin, H-Ti (Hydrogen-Titanium), in: F.D. Manchester (Ed.) Phase Diagrams of Binary Hydrogen Alloys, ASM International, Ohio, 2000, pp. 238-258.
[39] K.S. Forcey, D.K. Ross, C.H. Wu, The formation of hydrogen permeation barriers on steels by aluminising, Journal of Nuclear Materials, 182 (1991) 36-51.
[40] Saint-Gobain High-Performance Refractories:, Hexoloy® Silicon Carbide Materials, in, Saint-Gobain Ceramic Materials, 2018.
[41] M. Backhaus-Ricoult, Solid state reactions between silicon carbide and (Fe, Ni, Cr)-alloys: Reaction paths, kinetics and morphology, Acta Metallurgica et Materialia, 40, Suppl. (1992) S95-S103.
[42] R.C.J. Schiepers, J.A. van Beek, F.J.J. van Loo, G. de With, The Interaction between SiC and Ni, and Steel: Morphology and Kinetics, Journal of the European Ceramic Society, 11 (1993) 211-218.
[43] W.M. Tang, Z.X. Zheng, H.F. Ding, Z.H. Jin, A study of the solid state reaction between silicon carbide and iron, Materials Chemistry and Physics, 74 (2002) 258–264.
[44] K.S. Forcey, D.K. Ross, J.C.B. Simpson, D.S. Evans, Hydrogen transport and solubility in 316L and 1.4914 steels for fusion reactor applications, Journal of Nuclear Materials 160 (1988) 117-124.
[45] A.I. Gromov, Y.K. Kovneristyi, Permeability, diffusion, and solubility of hydrogen in Cr-Ni and Cr--Mn austenitic steels, Metal Science and Heat Treatment, 22 (1980) 321-324.
[46] E.H. Van Deventer, V.A. Maroni, Hydrogen permeation characteristics of some austenitic and nickel-base alloys, Journal of Nuclear Materials, 92 (1980) 103-111.
[47] T. Tanabe, Y. Yamanishi, K. Sawada, S. Imoto, Hydrogen transport in stainless steels, Journal of Nuclear Materials, 122 & 123 (1984) 1568-1572.
[48] E. Hashimoto, T. Kino, Hydrogen permeation through type 316 stainless steels and ferritic steel for a fusion reactor, Journal of Nuclear Materials 133 & 134 (1985) 289-291.
[49] D.M. Grant, D.L. Cummings, D.A. Blackburn, Hydrogen in 316 steel - diffusion, permeation and surface reaction, Journal of Nuclear Materials, 152 (1988) 139-145.
[50] T. Shiraishi, M. Nishikawa, T. Yamaguchi, K. Kenmotsu, Permeation of multi-component hydrogen isotopes through austenitic stainless steels, Journal of Nuclear Materials, 273 (1999) 60-65.
[51] A.D. LeClaire, Permeation of gases through solids: II. An assessment of measurements of the steady-state permeability of H and its isotopes through Fe, Fe-based alloys, and some commercial steels, Diffusion and Defect Data, 34 (1983) 1-35.
[52] High-Temperature characteristics of stainless steels, A designers' handbook series № 9004, in, distributed by Nickel development Institute, produced by American Iron and Steel Institute, http://www.nickelinstitute.org.

[53] T.P. Blach, E.M. Gray, Sieverts apparatus and methodology for accurate determination of hydrogen uptake by light-atom hosts, Journal of Alloys and Compounds, 446-447 (2007) 692-697.
[54] W.M. Mueller, Titanium Hydrides, in: W.M. Mueller, J.P. Blackledge, G.G. Libowitz (Eds.) Metal Hydrides, Academic Press, New York, 1968, pp. 336-383.
[55] T.R.P. Gibb Jr., H.W. Kruschwitz Jr., The Titanium-Hydrogen System and Titanium Hydride. I. Low-Pressure Studies, Journal of the American Chemical Society, 72 (1950) 5365-5369.
[56] C.C. Shen, T.P. Perng, Pressure–composition isotherms and reversible hydrogen-induced phase transformations in Ti–6Al–4V, Acta Materialia, 55 (2007) 1053-1058.
[57] A.D. McQuillan, The Titanium-Hydrogen System for Magnesium-reduced Titanium, Journal of the Institute of Metals, 79 (1951) 371-378.
[58] C.E. Buckley, E.M. Gray, E.H. Kisi, Stability of the hydrogen absorption and desorption plateaux in $LaNi_5$-H. Part 1: Hysteresis dynamics and location of the equilibrium isotherm, Journal of Alloys and Compounds, 215 (1994) 195-199.
[59] E.M. Gray, C.E. Buckley, E.H. Kisi, Stability of the hydrogen absorption and desorption plateaux in $LaNi_5$-H. Part 2: Effects of absorbing and desorbing large aliquots of hydrogen, Journal of Alloys and Compounds, 215 (1994) 201-211.
[60] D.P. Broom, C.J. Webb, Pitfalls in the characterisation of the hydrogen sorption properties of materials, International Journal of Hydrogen Energy, 42 (2017) 29320-29343.
[61] A.D. McQuillan, An Experimental and Thermodynamic Investigation of the Hydrogen-Titanium System, Proceedings of the Royal Society of London. Series A, Mathematical and Physical Sciences, 204 (1950).
[62] T. Førde, J. Maehlen, V. Yartys, M. Lototsky, H. Uchida, Influence of intrinsic hydrogenation/dehydrogenation kinetics on the dynamic behaviour of metal hydrides: A semi-empirical model and its verification, International Journal of Hydrogen Energy, 32 (2007) 1041-1049.
[63] Outotec Research Oy, HSC Chemistry, in, Chemistry Software, Pori, Finland, 2006.
[64] C.J. Webb, E.M. Gray, The effect of inaccurate volume calibrations on hydrogen uptake measured by the Sieverts method, International Journal of Hydrogen Energy, 39 (2014) 2168-2174.